Tensile mechanical behavior of as-cast AA7050 alloy in the super-solidus temperature range

T Subroto[1,2,*], A Miroux[1,2], D G Eskin[3], K Ellingsen[4], A Marson[5], M M'Hamdi[4], L Katgerman[2]

[1] Materials innovation institute (M2i), Mekelweg 2, Delft, 2628 CD, The Netherlands
[2] Dept. of Mat. Sci. and Engineering, Delft University of Technology, Mekelweg 2, Delft, 2628 CD, The Netherlands
[3] BCAST, Brunel University, Uxbridge, Middlesex, UB8 3PH, United Kingdom
[4] SINTEF Materials and Chemistry, NO-0314 Oslo, Norway
[5] SINTEF Materials and Chemistry, NO-7465 Trondheim, Norway
* Corresponding author: tsubroto@m2i.nl

Abstract Aluminum 7050 alloy is one of the primary alloys for the aviation industry owing to its excellent mechanical properties. However, this alloy has several poor physical properties that affect its solidification, such as relatively low thermal conductivity and large solidification range. These properties tend to increase the hot tearing susceptibility of the alloy, which makes it difficult to produce by direct-chill (DC) casting. Accurate knowledge of the mechanical behavior of the alloy during solidification is therefore crucial to ensure safe control of the casting process. Present work focuses on measuring the tensile mechanical properties of an as-cast AA7050 in the temperature range where hot tearing mainly occurs, i.e. from solid fractions of 0.85 to 1.0, or the solidus. Through these experiments, we extracted mechanical properties such as strain-rate sensitivity and ductility of the alloy in the super-solidus temperature range. The data obtained from this work will be useful in thermo-mechanical computer simulations aimed at reducing the hot tearing occurrence during DC casting, thus optimizing the production rate in the casting house.

Keywords AA7050, DC Casting, solidification, hot tearing, tensile mechanical properties

1. Introduction

AA7050 is one of the most used alloys for aerospace industries owing to its excellent mechanical properties such as high tensile strength, good fracture toughness and stress corrosion resistance [1, 2]. This alloy is usually produced via a vertical direct-chill (DC) casting method because of the robustness and relative simplicity of such process [3]. Despite its superior qualities, AA7050 is known to be susceptible to hot tearing due to its wide solidification range and relatively high thermal expansion coefficient [4]. Hot tearing usually occurs during DC casting, at the end of solidification when the alloy is in a semi-solid state but most of the liquid has been solidified and the remaining liquid resides at the grain boundaries [5]. The presence of such a defect causes the rejection of the ingot or lowers the quality of the cast product which subsequently affects its economical value [6]. In order to minimize the occurrence of hot tearing, it is critical to understand the mechanical properties in this solidification range [7]. Therefore, in this work, we investigated the tensile mechanical behavior of the alloy – which is the dominant stress mode related to hot tearing during DC casting, in the range of solid fractions of 0.85 and 1.0 (just before it is fully solidified), where hot tearing is most likely to occur. Such tensile mechanical properties will be useful input for a numerical process simulator aiming at minimizing the occurrence of hot tearing during DC casting, thus, optimizing the production rate in the aluminum cast house.

2. Experimental procedure

The tensile specimens used for the experiment were cut from an ingot produced via DC casting at Tata Steel (IJmuiden, The Netherlands). The ingot was DC cast using a conventional bore mold

from the melt that has been degassed in the furnace. The chemical composition of the alloy is given in Table 1.

Table 1. Chemical composition of AA7050.

Main alloying elements, wt pct					
Zn	Cu	Mg	Zr	Ti	Al
6.15	2.2	2.1	0.13	0.03	balance

The specimens were tested using a set-up developed at SINTEF Materials and Chemistry with an Instron 5944 series tensile test machine equipped with a 2-kN load cell. The specimen was heated up using an induction heating coil system which was controlled by a Eurotherm™ temperature controller. A quartz-glass tube coated with boron nitride aerosol on the inside, was used to enclose the center part of the sample in order to avoid liquid breakout during the fully melt phase. The coating was intended to prevent the sticking of the liquid aluminum onto the quartz tube which might affect the force measurement due to the added friction resistance. The experimental cycle (for both re-melt and mechanical testing temperature) is shown in Figure 1.

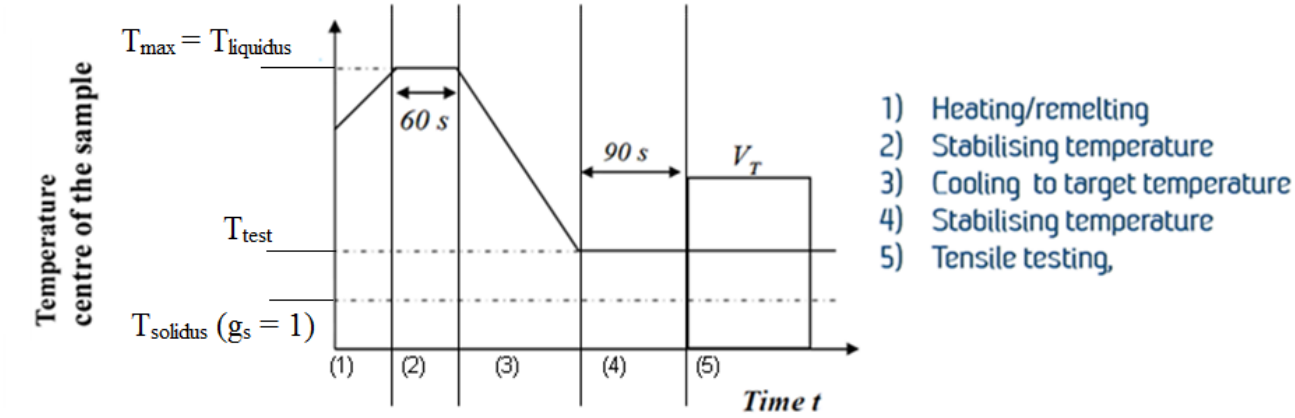

Figure 1. Experimental cycle of the tensile test.

The test cycle that we used in our experiment was as follows. First, we heated up the sample from room temperature up to T_{max} = 635 °C, which is the liquidus of an AA7050 alloy based on the JMat-Pro software (Figure 2). Then we held the sample at T_{max} for 60 seconds to assure that the central part of the specimen is fully liquid. Subsequently, we cooled down the sample to the test temperature with a cooling rate of 1 °C/s. We then held the sample at this test temperature for approximately 90 seconds to let the temperature in the specimen stabilize. Then we performed the mechanical tensile testing of the sample at a certain displacement rate until the force value was approximately zero after the fracture.

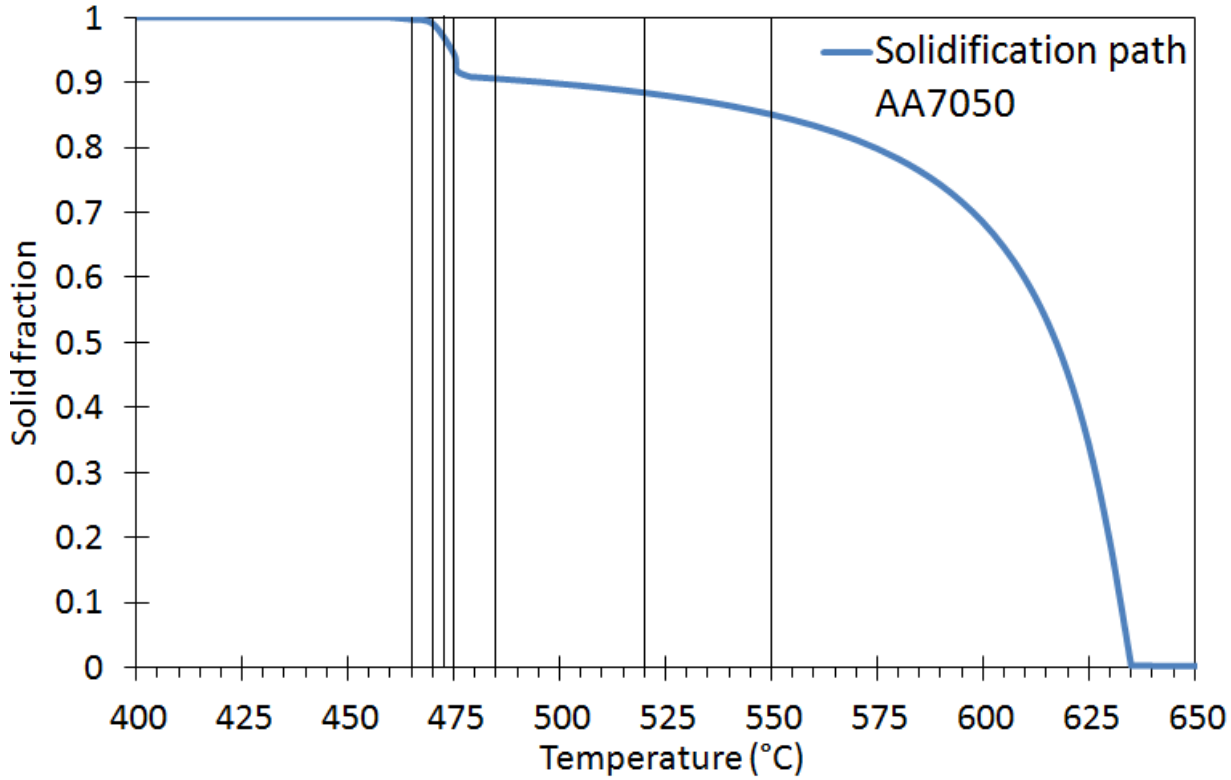

Figure 2. The solidification path of an AA7050 alloys as calculated by JMat-Pro software (Scheil calculation).

The test temperatures that we used in this work corresponded to solid fractions (f_s) between 0.85 and 1.0. We took data at several points within this range such as at 0.85, 0.88, 0.9, 0.94, 0.97, 0.99 and 1.0 or in terms of temperature – at 550, 520, 485, 475, 473, 470 and 465 °C, respectively. The solidification path of this alloy was calculated by JMat-Pro software and is shown in Figure 2, the vertical lines in such a figure show the temperature points where we performed the data acquisitions. To observe the displacement-rate sensitivity behavior of the alloy in this temperature range, we used two different displacement rates. For each combinations of the test (temperature–displacement rate), we repeated the test three to four times to obtain statistical information of the test. The fracture surface of the samples was observed in a Jeol JSM-6500F scanning electron microscope (SEM) at the tip of the failed specimens.

3. Results and discussion

3.1 Mechanical properties

From the tensile tests, we obtained force–displacement curves at different temperature points and displacement rates. The force–displacement curves with a displacement rate of 0.2 mm/min are shown on Figure 3 and with a displacement rate of 2 mm/min, on Figure 4. Due to the large scaling range of the force value, at the displacement rate 0.2 mm/min, we divided the entire data into two sets: The data from f_s = 1.0 down to f_s = 0.97 are shown in Figure 3a and the data from f_s = 0.97 down to f_s = 0.85 are shown in Figure 3b.

Figure 3 shows that at the displacement rate 0.2 mm/min, the height of the peak force in general

decreases as the solid fraction reduces. In addition, the shape of the curve also changes quite significantly from f_s = 1.0 (when the alloy is fully solid) to f_s = 0.97 (refer to Figure 3a) and then it changes again as the solid fraction decreases further, from f_s = 0.97 down to f_s = 0.85 (refer to Figure 3b). Such a transition in the force–displacement curve can be interpreted as a change in the mechanical behavior regime. From Figure 3, we observed two mechanical properties transitions. First, when the alloy behavior changes from ductile at f_s = 1.0 to brittle at f_s = 0.97. The sharp drop in ductility and strength at f_s = 0.97 informs us that the alloy fails in a brittle manner. The second transition in the mechanical behavior of the material occurs when the solid fraction of the alloy decreases from f_s = 0.97 to f_s = 0.85. As the solid fraction decreases, the end part of the curve (after peak force) changes, i.e. the slope of the curve is not as steep as for f_s = 0.97 and the slope gradually becomes shallower as the solid fraction decreases. Finally at the lowest solid fraction in this test (f_s = 0.85), the curve resembles a shallow symmetric hump with a long 'tail'. This might be caused by the sufficient liquid presence in the alloy, thus it is as if the alloy is dragging viscous liquid. Another possible explanation is, as suggested by Eskin *et al.* [8], that the main mechanism of deformation is grain boundary sliding thanks to the presence of sufficient interdendritic liquid surrounding the grain at such solid fraction.

Similar force–displacement curve shape change is also observed at a displacement rate of 2 mm/min. As shown in Figure 4, at f_s = 0.99, the force exhibits a sharp drop after the sample reaches fracture point which is interpreted as a brittle behavior of the alloy. As solid fraction decreases to f_s = 0.94, the peak force significantly decreases despite the similar curve shape with the preceding case. The main shape distinction is that the curve at f_s = 0.94 has a 'tail' after the sharp drop, which could be explained due to the additional amount of liquid at such solid fraction as compared to the higher solid fraction. At f_s = 0.90, the peak force is reduced even more and the shape of the force–displacement curve is significantly changed as compared to the two other curves at this displacement rate.

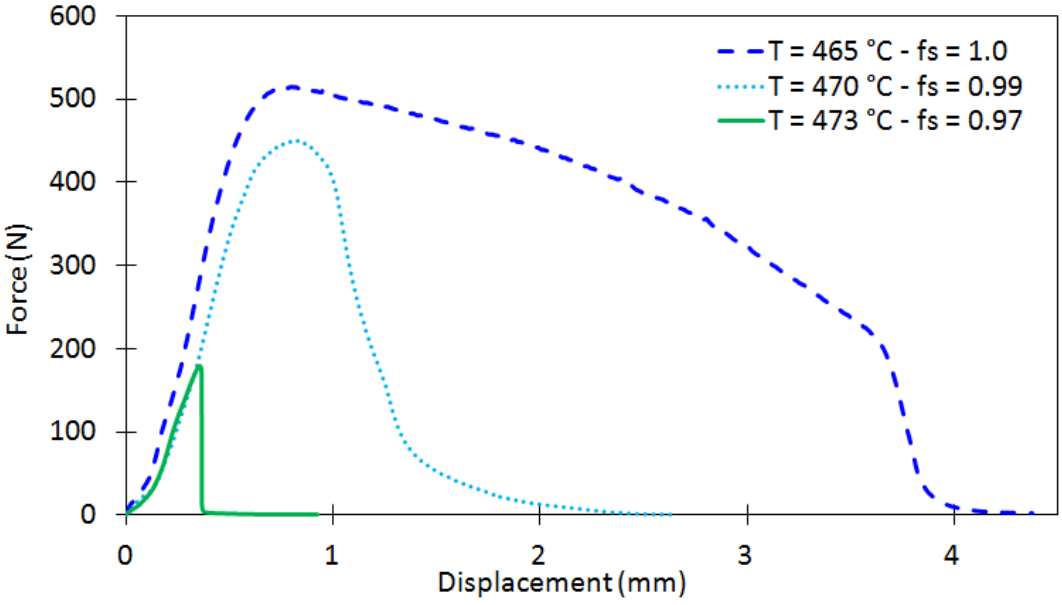

(a)

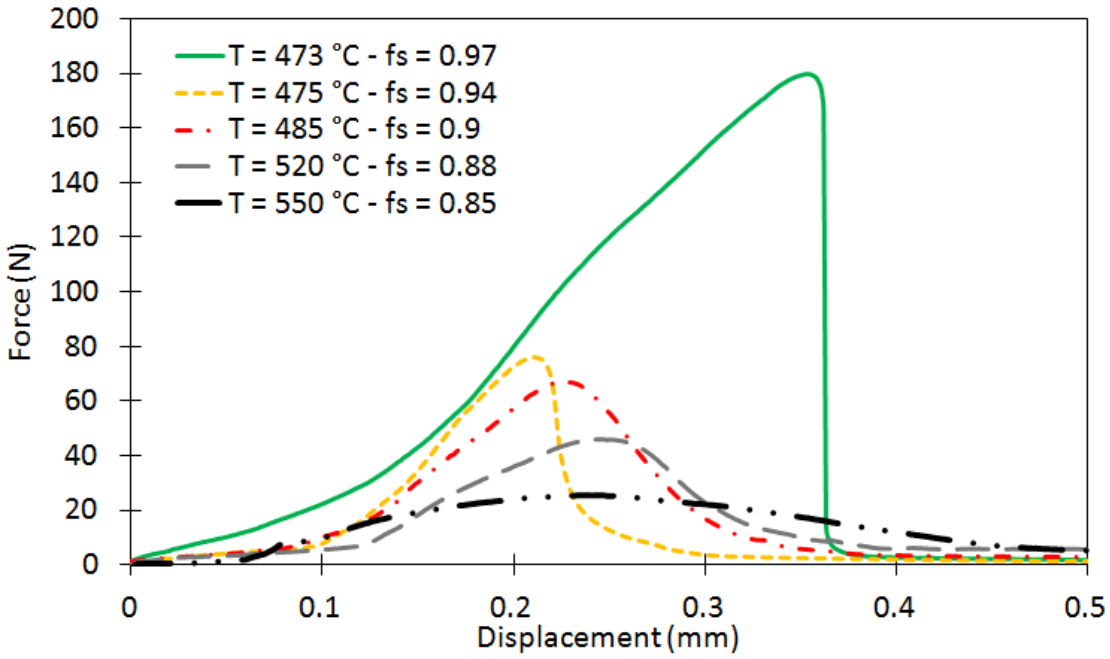

(b)

Figure 3. Force–displacement curves at a displacement rate of 0.2 mm/min for the solid fraction ranges from $f_s = 1.0$ – fully solid to $f_s = 0.97$ (a) and from $f_s = 0.97$ to $f_s = 0.85$ (b).

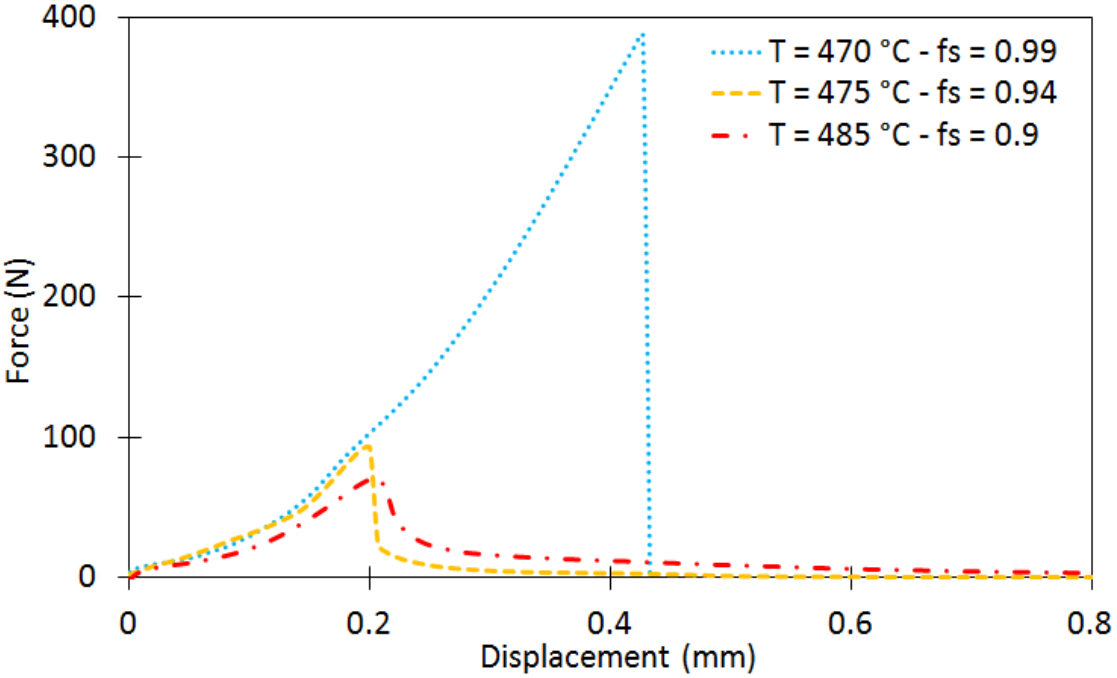

Figure 4. Force–displacement curves at a displacement rate of 2 mm/min for solid fractions from $f_s = 0.99$ to $f_s = 0.9$.

The evolution of the peak force of the alloy with respect to the temperature is shown in Figure 5. For both displacement rates, the peak force rapidly increases as the temperature is lowered below 475 °C. Therefore, we can argue that the grain coalescence occurs between $f_s = 0.94$ and $f_s = 0.97$. These values are supported by a few other works on different alloys [9, 10]. The temperature range

from 475 to 470 °C also coincides with the brittle fracture behavior and the eutectic solidification domain. One can also notice that the alloy starts to become sensitive with respect to displacement rate, the largest sensitivity at the lowest temperatures. In addition, one can observe that the error bars (standard deviation) are larger when the sample becomes brittle and smaller if it is ductile.

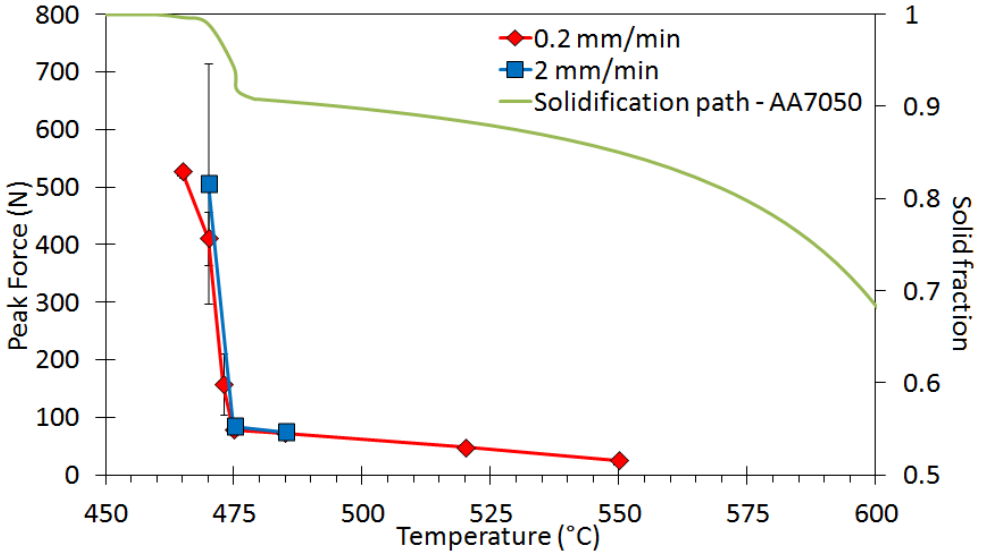

Figure 5. Comparison in peak forces between two different displacement rates at different temperature points (left vertical axis) and corresponding solid fractions (right vertical axis). The error bars are shown; when not visible they are smaller than the size of the data point.

The ductility of the alloy at different temperature points is shown in Figure 6. For both displacement rates, one can see that the ductility of the alloy starts to drop significantly as the temperature increases above 465 °C. The lowest ductility value for both displacement rates was found at a temperature of 475 °C or f_s = 0.94, which corresponds, according to the solidification path in Figure 2, to the beginning of the eutectic solidification. As the temperature increases further above 475 °C, the ductility starts to develop gradually up to 550 °C. If extrapolated to higher temperatures, the temperature dependence of the ductility points would resemble the shape of the classical brittle temperature range curve [8].

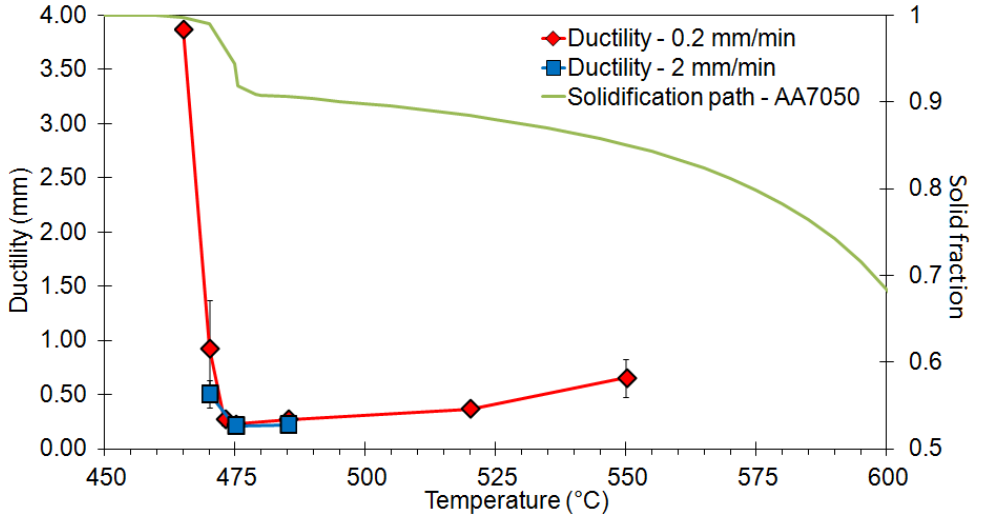

Figure 6. Comparison of the ductility of the alloy at different temperature points (left vertical axis) with respect to its respective solid fraction of the alloy (right vertical axis).

The displacement rate has a small effect on the mechanical behavior. The main difference is that at 470 °C the four tests at 2 mm/min gave a brittle behavior while at 0.2 mm/min two tests showed a brittle behavior the other two giving a ductile response. At temperature of 475 °C, there is a slight change in curve shape with different displacement rates. The most significant change is the shape of the curve after the peak force was reached. At lower displacement rate, the decrease is more gradual compared to the slope at 2 mm/min. This behavior is reasonable, because at 0.2 mm/min, the alloy has more time to compensate the deformation.

3.2 Fracture surface analysis

To analyze the behavior during fracture, we performed SEM analysis of the fracture surfaces at four different conditions, i.e. at two deformation rates and at solid fractions of 0.99 and 0.94, reflecting the transition from brittle to ductile behavior (see Figures 3–5). From all of the fracture analysis performed, we found that in general, the fracture mode is mixed between inter-granular (with dendritic morphology) and intra-granular. We observed such a mixed fracture mode at both solid fractions and displacement rates (figure 7). Moreover, features that possibly attest for broken dendrite arms (features within the dashed white ellipses in Figure 8a) were found for all conditions.

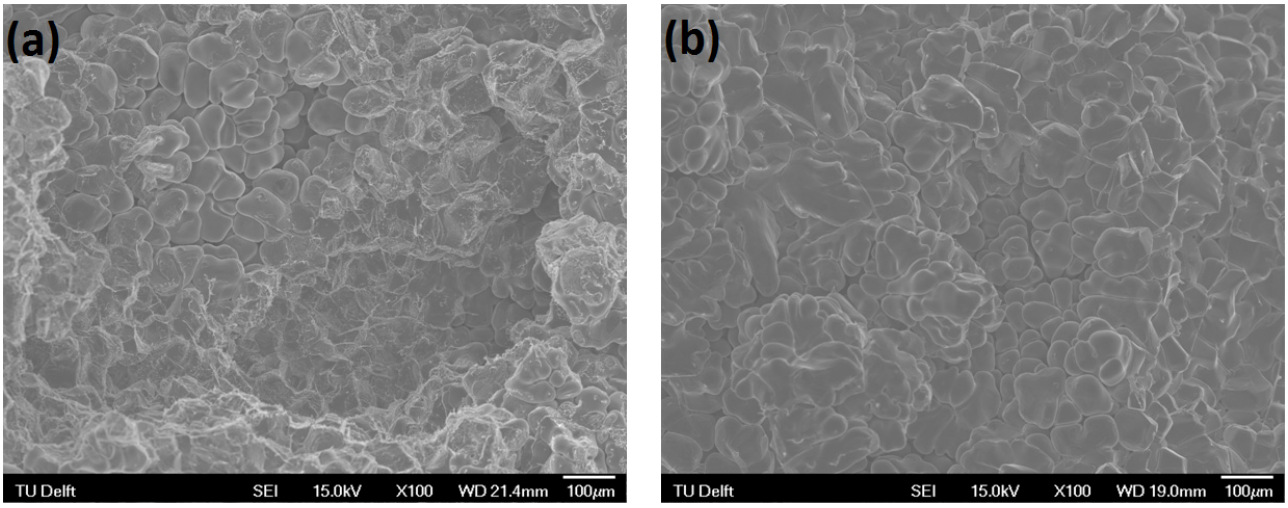

Figure 7. Examples of mixed-mode fracture surface at $f_s = 0.99$ with 0.2 mm/min displacement rate (a) and $f_s = 0.94$ with 2 mm/min displacement rate (b).

The higher solid fraction ($f_s = 0.99$) and lower displacement rate (0.2 mm/min) shows deformation of the solid and interdendritic liquid phases as evidenced in Figure 8b. While with a higher displacement rate (2 mm/min) and same solid fraction the interdendritic liquid phases have different shape (Figure 8c). The shape differences could be explained as the interdendritic liquid has more time to deform and rearrange at lower displacement rate compared to the higher one. At lower solid fraction ($f_s = 0.94$), for both displacement rates, the interdendritic liquid raptures [11] (features within the dashed white ellipses in Figure 8d) and the solid bridges fracture in a brittle fashion as illustrated in Figure 8d. Interestingly, such interdendritic liquid features are rarely found at the higher solid fraction.

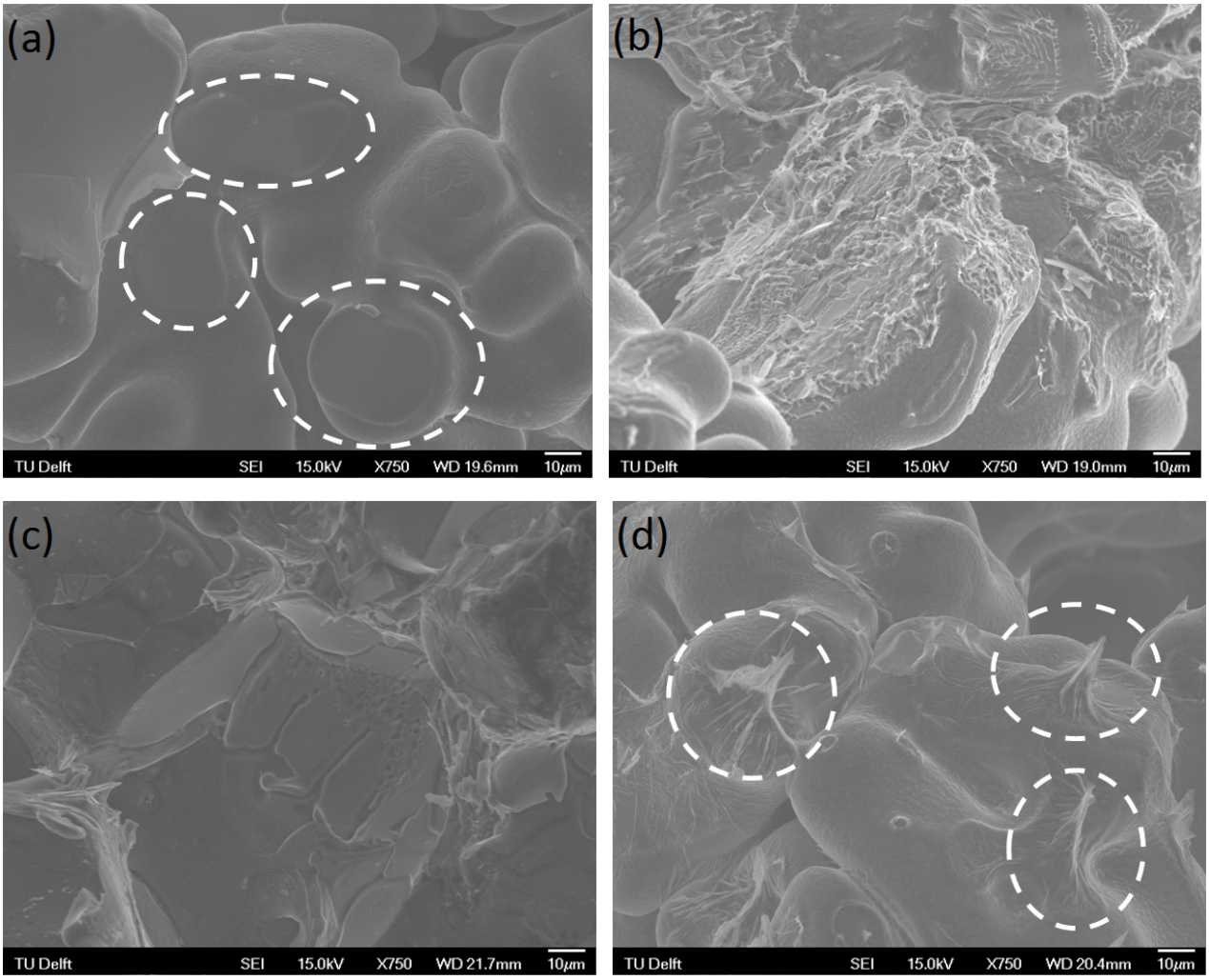

Figure 8. Pictures of fracture surface analysis using SEM: (a) Examples of broken dendrite arms, (b) example of extra-deformed eutectics, (c) example of layer-like eutectics and (d) examples of features that resemble necking of the interdendritic liquid stretched during fracture.

4. Summary

We can summarize the results obtained from the experiments as follows:

1. From the shape of the force–displacement curves, we found that in the range of f_s = 1.0 (fully solid) to f_s = 0.85, the alloy has three different mechanical behavior regimes; ductile (between f_s = 1.0 and f_s = 0.99), brittle (between 0.99 and 0.9) and then ductile again (between 0.9 and 0.85).
2. The grain coalescence in AA7050 occurs between f_s = 0.94 and f_s = 0.97. This is showed by the sharp increase in peak force between the mentioned solid fractions.
3. The alloy has almost no displacement rate sensitivity at high temperatures (below f_s = 0.94) but it has positive displacement rate sensitivity starting at f_s = 0.94 and at higher solid fractions.
4. The alloy produces a ‘classically’ shaped brittle temperature range curve with the minimum of ductility reached at 475 °C, and the alloy gains again ductility as the liquid fraction increases in the alloy.
5. From SEM fracture surface analyses at different data points showed in Figure 7, it is found

that in general the fracture mode is mixed between inter- and intra-granular. Additionally, at higher solid fraction, the morphology of eutectic is different at different displacement rates (Figure 8b and 8c). Sites that resemble necking of interdendritic liquid was observed at samples that were tested at lower solid fraction (Figure 8d), independent of displacement rate used during the test.

Acknowledgment

This research was carried out within the Materials innovation institute (www.m2i.nl) research framework, project number M42.5.09340. The establishment of the experimental set-up and testing procedure for the mechanical tensile testing in the semi-solid has been supported by the Norsk Hydro Fond for SINTEF. The authors would like to express their gratitude to Dr. Démian Ruvalcaba and Mr. Jacob van Oord (Tata Steel Research, Development & Technology, The Netherlands) and also to Mr. Hans I. Lange and Mr. Arne Nordmark (SINTEF Materials and Chemistry, Norway) for their support and inputs. Support from Modelling assisted INnovation for Aluminum DC Casting process (MINAC) community is highly appreciated.

References

[1] J.C. Williams, E.A. Starke Jr, Acta Materialia, 51 (2003) 5775-5799.
[2] L. Schra, W.G.J.t. Hart, Engineering Fracture Mechanics, 17 (1983) 493-507.
[3] M. Lalpoor, D.G. Eskin, L. Katgerman, Materials Science and Engineering A, 497 (2008) 186-194.
[4] M. Lalpoor, D.G. Eskin, L. Katgerman, Metallurgical and Materials Transactions A: Physical Metallurgy and Materials Science, 41 (2010) 2425-2434.
[5] D. Fabrègue, A. Deschamps, M. Suéry, W.J. Poole, Metallurgical and Materials Transactions A: Physical Metallurgy and Materials Science, 37 (2006) 1459-1467.
[6] A.B. Phillion, S.L. Cockcroft, P.D. Lee, Acta Materialia, 56 (2008) 4328-4338.
[7] M. Suéry, in: Conference of Advances in Metallic Materials and Manufacturing Processes for Strategic Sectors, 2012, pp. 35-42.
[8] D.G. Eskin, Suyitno, L. Katgerman, Progress in Materials Science, 49 (2004) 629-711.
[9] O. Ludwig, J.M. Drezet, C.L. Martin, M. Suéry, Metallurgical and Materials Transactions A: Physical Metallurgy and Materials Science, 36 (2005) 1525-1535.
[10] O. Ludwig, J.M. Drezet, P. Ménésès, C.L. Martin, M. Suéry, Materials Science and Engineering A, 413-414 (2005) 174-179.
[11] M. Rappaz, J.M. Drezet, P.D. Grasso, A. Jacot, in: 10th Modeling of Casting, Welding and Advanced Solidification Processes (MCWASP X), 2003, pp. 53-60.